

DFT modelling of stacking faults in hexagonal and cubic GaN

Zijie Wang*

*Dept. Physics & Astronomy, University College London,
Gower Street, London, WC1E 6BT, United Kingdom. and
London Centre for Nanotechnology, University College London,
17-19 Gordon Street, London, WC1H 0AH, United Kingdom.*

Mazharul M. Islam†

*London Centre for Nanotechnology, University College London,
17-19 Gordon Street, London, WC1H 0AH, United Kingdom.*

David R. Bowler‡

*London Centre for Nanotechnology, University College London,
17-19 Gordon Street, London, WC1H 0AH, United Kingdom.
Research Centre for Materials Nanoarchitectonics (WPI-MANA),
National Institute for Materials Science (NIMS),
1-1 Namiki, Tsukuba, Ibaraki 305-0044, Japan and
Dept. Physics & Astronomy, University College London,
Gower Street, London, WC1E 6BT, United Kingdom.*

(Dated: January 19, 2026)

We have performed density functional theory (DFT) calculations to characterize the energetics, and the atomic and electronic structure, of stacking faults in GaN, both in the stable hexagonal wurtzite (wz) phase and in the metastable cubic zincblende (zb) phase. In wz GaN, SFs on the (0001) planes can be divided into three different intrinsic stacking faults (I_1 , I_2 , and I_3) and one extrinsic stacking fault (E). In zb GaN, SFs form along (111) directions, giving one type each of intrinsic, extrinsic and twin SFs. Based on the calculated formation energy, I_1 is the most stable SF of wz GaN in agreement with experiment. For zb GaN, the intrinsic stacking fault is the most dominant planar defect. To characterize the effect of the stacking faults on the electronic structure of the material, we examined the band density. We found that the bands near the valence band maximum in wz GaN are localised on the Ga-polar side of the stacking fault (i.e. on the Ga side of the Ga-N bonds perpendicular to the SF), with the bands near the conduction band minimum more on the N-polar side, though somewhat delocalised. We found the opposite trend in zb GaN; this behaviour is caused by a redistribution of charge near the interface. We also show the band offsets for the stacking faults, finding that they are very sensitive to local conditions, but can all be described as type II interfaces, with the presence of a stacking fault reducing the gap locally.

I. INTRODUCTION

III-V nitrides are increasingly important in electronic and optoelectronic devices [1, 2]. These applications are affected by a number of material problems, mostly due to the lack of suitable substrates on which the materials are grown. Growth on mismatched substrates causes the epilayers to contain a very high concentration of extended defects, i.e., stacking faults, up to five orders of magnitude higher than in other materials used for optoelectronic devices [3]. Although most commercial GaN devices are based on the stable *c*-oriented wurtzite (wz) GaN, these materials present a strong piezoelectric effect in the [0001] direction [4]. As a result of this phenomenon, band bending occurs through the quantum confined Stark effect [5, 6].

Through epitaxial growth of GaN films on cubic sub-

strates, a metastable cubic zincblende (zb) structure can be stabilized [2, 7], which is not polar like the wz phase, reducing the issues for optoelectronic devices. Recent studies show that, due to the absence of polarization fields and the lower band gap compared to wz GaN, zb GaN shows higher efficiency in longer wavelength emission (green, amber, red) [8]. The stacking faults in zb GaN can be treated as wz insertions in a zb matrix [8] which modify the optical properties of cubic GaN films and propagate into active layers. In quantum wells and electron blocking layers, the segregation of alloying elements has been observed at stacking faults, leading to the formation of quantum wires and polarized emission [9]. The SFs have been shown to facilitate electronic confinement and induce spontaneous ordering in p-type systems [10, 11].

Many questions have yet to be answered concerning the high resolution characterization of SFs' densities, alloy segregation to SFs and their influence on the optoelectronic properties of GaN-based devices. The density of stacking faults in basal (0001) planes were measured with x-ray diffraction (XRD) [4]. High resolution trans-

* ucapzw4@ucl.ac.uk

† ucanmmi@ucl.ac.uk

‡ david.bowler@ucl.ac.uk

mission electron microscopy (TEM) helped to understand zb/wz heterostructures, which result from the spontaneous polarization of wz GaN [12]. Recently, a combination of high-resolution scanning transmission electron microscopy (STEM) and energy dispersive x-ray spectrometry was used to investigate the effects of alloy segregation around stacking faults in a zb GaN light-emitting structure [13]. A key question remaining is to identify the change in atomic spacing at the SFs, and whether this plays a significant role in segregation phenomenon [9]: here, atomistic modelling can complement experiments, and provide insights beyond experimental resolution. DFT modelling has previously focused on the energetics and electronic structure of basal stacking faults of wz GaN [14–16] with forcefield modelling considering energetics in zb GaN [17]. However, there have been no DFT studies on SFs in zb GaN, and a detailed examination of the effects of stacking faults on the local electronic structure and band edges has not been performed.

In this paper, our aim is to study the atomic structure and energetics of SFs, alongside their electronic structure and differences to bulk material in both wz and zb phases of GaN, and to compare to recent high-resolution STEM imaging of those SFs [13, 18]. The rest of the paper is laid out as follows: in Sec. II, the computational approach is presented; the results for the structural and energetic properties are compared in Sec. III; the electronic structure of the SFs is discussed in Sec. IV; Sec. V gives a brief summary and concludes the paper.

II. COMPUTATIONAL METHODS AND MODELS

In this work, calculations were performed using Density Functional Theory (DFT) as implemented in the CONQUEST code which is designed for large-scale, massively parallel simulations on thousands to millions of atoms[19–21]. The DFT calculations used the generalized gradient approximation (GGA) based Perdew–Burke–Ernzerhof (PBE) exchange-correlation functional [22]. Core electrons were modeled using Hamman’s optimised norm-conserving pseudopotentials [23] from the PseudoDojo database[24], while valence electrons were represented by real-space local orbital basis functions, specifically pseudo atomic orbitals (PAOs) [25] at the double-zeta plus polarization (DZP) level. The PAOs were generated using the equal radii approach, with details given in the Supporting Information (SI). The real-space integration grid spacing was set to be equivalent to a 400 Ha kinetic energy, or 0.1 Bohr, which converges total energies to better than 1 μ Ha and stresses to better than 0.01 GPa.

The structural relaxation was performed in two steps. First, the simulation cell was optimized to a tolerance of 0.1 GPa using the conjugate gradient algorithm, with fixed fractional ionic coordinates; to mimic the effects of a fixed substrate, only the stress along c was minimised,

with values of a and b fixed to bulk parameters. The stabilized quasi-Newton method (SQNM)[26] was then used to optimize the ionic positions with a threshold of 0.02 eV \AA^{-1} .

The wurtzite structure, which is hexagonal, is characterized by a stacking sequence of repeating layers AB along the (0001) direction[27]. However, as CONQUEST supports only orthorhombic cells, we must use a cell where we constrain the b/a ratio to maintain the correct shape (in the simplest cell, the ratio is $\sqrt{3}$). The orthorhombic wz GaN simulation cell contains eight atoms, which we modelled using a $9 \times 6 \times 6$ gamma-centred Monkhorst–Pack k-point mesh; this gives convergence of total energy to around 10 μ Ha and stress to around 0.01 GPa. The zincblende phase is cubic and can be characterized by a stacking sequence of repeating layers ABC along the (111) direction. For the calculations of stacking faults and to simplify comparison with the wurtzite structure, we used a simulation cell oriented along the (111) direction of the cubic cell. We again constrain the b/a ratio to $\sqrt{3}$ to maintain the correct crystal geometry. The resulting simulation cell contains twelve atoms, which we modelled using a $9 \times 6 \times 3$ gamma-centred Monkhorst–Pack k-point mesh. The optimised lattice parameters agree well with experiment and previous DFT studies, and are given in the SI, along with lattice parameters for InN and AlN.

The formation energy per unit area of the simulation cell for the optimized SFs is calculated as:

$$\Delta E = E_{SF} - nE_{Ref} \quad (1)$$

where E_{SF} is the total energy of the specific SF in a simulation cell containing n layers, and E_{Ref} is the energy per layer of the host material.

When considering band offsets between perfect bulk cells and cells with stacking faults, we need a common zero. The semi-core d electrons in Ga form a natural low-lying band which allows comparison; however there are two groups of low-lying d bands separated by around 1.9 eV, with the lowest energy band showing dispersion of around 0.7 eV, while the upper group of d bands show dispersion of less than 0.1 eV. This upper group forms a suitable reference point to compare the energies of different sets of bands, and we choose the value at the gamma point to set the common zero.

III. PHYSICAL STRUCTURE AND ENERGETICS

Taking the optimized lattice parameters and atomic coordinates of bulk structures, a series of simulations cells was constructed containing stacking faults, with progressively increasing separation between the stacking faults to test the convergence. For wz GaN, the three intrinsic stacking faults I_1 , I_2 , I_3 in isolation would be formed as \dots AB/CB \dots , \dots AB/CA \dots and

...AB/C/BA... respectively. When modelled with periodic boundary conditions some adjustment is required, and we need two stacking faults in each cell. For n layers of each stacking sequence, we then have /nAB/nCB/, /nAB/nCA/C/ and /nAB/C/nBA/C/ where the stacking faults are in the middle and at the edges of the cell, and an extra C layer has been added to both I_2 and I_3 to restore periodicity. For the extrinsic stacking fault, we have ...AB/C/AB... in isolation, and /nAB/C/ in a periodic cell (in this case, we need only one stacking fault per simulation cell).

For zb GaN, in isolation, the intrinsic, extrinsic and twin stacking faults are formed as ...ABC/BC/ABC..., ...ABC/B/ABC... and ...ABC/BAC/ABC... respectively. We can accommodate a single stacking fault in a periodic cell in all three cases, which for n layers we write as /nABC/BC/, /nABC/B/ and /nABC/BAC/ in each case. These models are illustrated in Figs. 1 and 2.

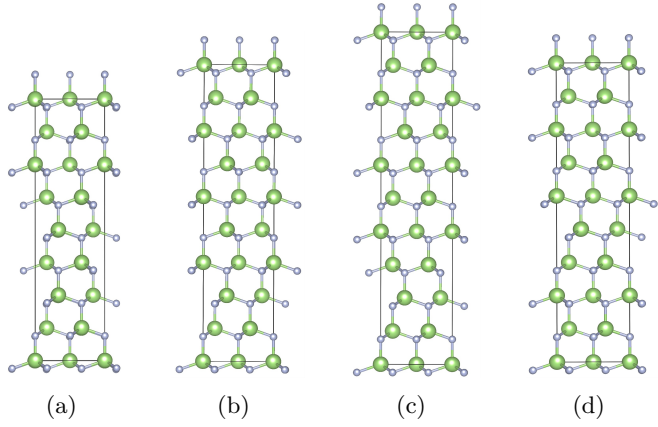


FIG. 1: Stacking faults in wurtzite GaN. (a) Intrinsic 1 (I₁) /AB/CBCB/AB/, (b) Intrinsic 2 (I₂) /AB/CACA/C/AB/, (c) Intrinsic 3 (I₃) /AB/C/BABA/C/AB/ and (d) Extrinsic /ABAB/C/ABAB/. Note that these are highly shortened cells for illustration only.

We tested the effect of increasing the number of layers of bulk material between stacking faults in both wz and zb, to find the converged value of the formation energy, which we give in mJ/m^2 . The converged values are given in Table I along with number of layers. Full details of the convergence of the energy with number of layers are given in the supplementary information. Based on these calculated formation energies, SFs in wz GaN all show a positive energy, with I_1 being the most stable SF. This agrees well with the experimental observation that 90% of observed basal plane stacking faults in wz GaN films are of I_1 -type [28, 29]. The second most common SF is I_2 followed by I_3 and E; experimentally, the extrinsic type of SF is rarely observed [30]. The observed trend is in good accord with energies calculated in other DFT investigations [14–16] though none of these studies report details of convergence tests of spacing between SFs.

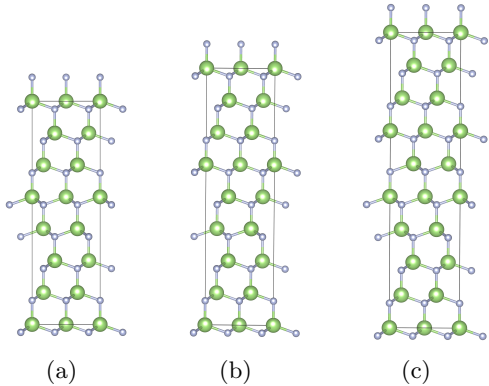


FIG. 2: Stacking faults in Zincblende GaN. (a) Extrinsic /ABC/B/ABC/, (b) Intrinsic /ABC/BC/ABC/ and (c) Twin /ABC/BAC/ABC/. Note that these are highly shortened cells for illustration only.

In zb GaN, however, all stacking faults have a negative formation energy; this is not surprising, as SFs represent a small wz inclusion in the zb lattice, and wz is the more stable crystal. All of the SFs have almost the same energy (certainly the difference between them is within the accuracy limit of these calculations) though the experimental observation is that the intrinsic stacking fault (SF) is the most abundant planar defect in epitaxial layers [9].

All stacking faults have a very low formation energy, implying that these defects may form very easily in both wz and zb GaN, though they are much more likely to form in the zb phase.

TABLE I: Calculated values of formation energy (mJ/m^2) of stacking faults (ΔE) and converged number of layers (N) for wz (upper) and zb (lower) phases of GaN.

Wurtzite GaN			
I ₁	I ₂	I ₃	E
ΔE	17	28	36
N	24	33	34
Zincblende GaN			
I	E	T	
ΔE	-33	-34	-34
N	26	25	27

Accurate determination of the stacking fault thickness (l) is essential for calculating the band profile of stacking faults functioning as quantum wells (QWs) [8]. The calculated stacking-fault thickness l for the optimized models of all the considered types of SFs are provided in Table III. Here we use the inter-planar spacing as discussed in a recent experimental investigation based on combined high-resolution scanning transmission electron microscopy and energy dispersive x-ray spectrometry

try [9]. At 300 K, the c lattice parameter of bulk wz GaN and the lattice parameter of bulk zb GaN are measured to be 5.186 Å and 4.506 Å, respectively, corresponding to inter-planar spacings of 2.593 Å and 2.602 Å in wz-GaN and zb-GaN [31–33]. Bulk zb-GaN exhibits a larger inter-planar spacing between close-packed planes compared to bulk wz-GaN, which may be attributed to stronger Coulombic interactions between third-nearest-neighbor Ga and N atoms in the wurtzite phase. Our calculated lattice parameters for the bulk wz GaN are $a = 3.235$ Å and $c = 5.284$ Å and for bulk zb GaN, it is $a = 4.578$ Å. The resulting inter-planar spacing $d(0001)$ in bulk wz-GaN is 2.642 Å and $d(111)$ in bulk zb-GaN is 2.644 Å. These show good agreement with the experimental measurements[31–33] though perhaps the difference between the phases is a little small. SFs can be seen as small insertions into the crystal of the other crystal type, and their equilibrium inter-planar spacing may, thus, be similar to the inter-planar spacing in the non-defective materials. In Table III, the calculated largest (l_{max}) and smallest (l_{min}) distances of the SFs are presented. Our calculated stacking faults thicknesses range from 2.639 to 2.643 Å for wz GaN and 2.643 to 2.644 Å for zb GaN, showing a very small variation; plots of the evolution of the layer spacing along the c axis of the simulation cell are given in the supporting information. (The alternative approach to define SF thickness using multiples of the Ga-N bond length [16, 34] gives similar insight but with less detail, so we do not use it.)

TABLE II: Calculated range of layer spacings in stacking faults with respect to ideal crystals of wz and zb GaN.

Stacking faults based on Wurtzite GaN				
Bulk	I ₁	I ₂	I ₃	E
2.642	2.640–2.643	2.640–2.643	2.639–2.643	2.640–2.642
Stacking faults based on Zincblende GaN				
Bulk	I	E	T	
2.644	2.643–2.644	2.643–2.644	2.643–2.644	

IV. ELECTRONIC STRUCTURE

It is important to characterise the effect of the stacking faults on the electronic structure of the materials (both wz and zb GaN). While SFs can be seen as simply a change in the layer ordering, they can also be seen as a small inclusion of the other crystal (i.e. zb in wz and vice versa) which will involve a change from polar to non-polar (or vice versa) material, with potentially significant effects on the electronic structure.

In the first instance, we plot band resolved densities to visualise the changes around the Fermi level in real-space. In the usual way, we define the density for band n as $\rho_n(\mathbf{r}) = \sum_{\mathbf{k}} w_{\mathbf{k}} |\psi_{n\mathbf{k}}(\mathbf{r})|^2$ where $w_{\mathbf{k}}$ is the weight

for each point in the Brillouin zone. The band densities show similar trends for all SFs in each material, so we show here the bands for the most common SF in wz (I₁) in Fig. 3 and in zb (I) in Fig. 4. Band densities for all other SFs are given in the supporting information.

In both wz and zb the bands near the top of the valence band (Fig. 3(a)-(d) in wz and Fig. 4(a)-(d) in zb) are localised on one side of the SF, and the bands near the bottom of the conduction band (Fig. 3(e)-(h) in wz and Fig. 4(e)-(h) in zb) are localised on the other side (though this is perhaps a little clearer in zb). Similar behaviour is seen in all other stacking faults in both materials.

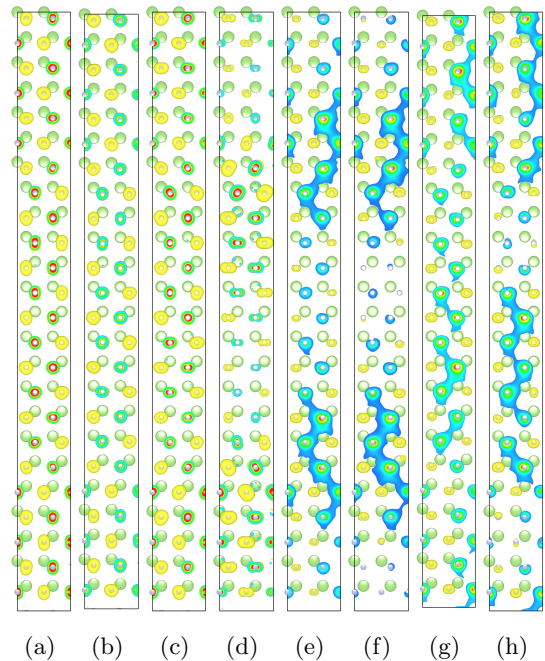


FIG. 3: Band resolved densities of Intrinsic-1 stacking fault of wz GaN, here shown with six layers between stacking faults (/3AB/6CB/3AB/). The bands below the Fermi energy are shown in panels (a-d), and the bands above the Fermi energy are shown in panels (e-h). The isosurfaces were plotted at a density of 0.0005 electrons per Bohr³. Note that there are two stacking faults in the simulation cell, 25% and 75% of the way along the cell.

However, the localisation occurs on different sides of the SF in wz and in zb: in wz, the valence bands are localised on the Ga-polar side of the stacking fault (i.e. on the Ga side of the Ga-N bonds perpendicular to the SF, or below the stacking fault as plotted) with the conduction bands localised on the N-polar side. By contrast, in zb the opposite trend is seen, with the valence bands on the N-polar side of the SF (above the stacking fault as plotted) and conduction bands on the Ga-polar side (below the stacking fault as plotted).

We seek to identify the mechanism underlying this localisation of the bands on one side of the SF, and the origin of the difference between the different behaviour in

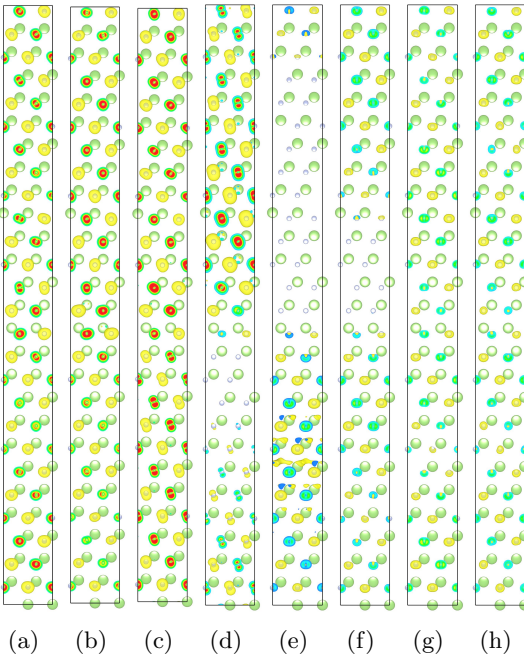


FIG. 4: Band resolved densities of Intrinsic stacking fault for zb GaN along (111), here shown with eight layers between stacking faults (/4ABC/BC/4ABC/). The bands below the Fermi energy are shown in panels (a-d), and the bands above the Fermi energy are shown in panels (e-h). The isosurfaces were plotted at a density of 0.0005 electrons per Bohr³. There is one stacking fault, halfway along the simulation cell.

the two materials. We characterise the problem by comparing the electrostatic potential in the faulted material with perfect material, and consider the potential along the *c*-axis of the simulation cell, taking a planar average in the *a*–*b* plane. The resulting potential trace is shown for the most stable SFs in the top panels of Fig. 5(a) and (b) for wz and zb respectively (we again show plots for all other SFs in the supplementary information).

We see that the potential changes rapidly across the SFs in both materials (noting that there are *two* SFs in the wz simulation cell) with periodicity leading to a slow variation of the potential across the rest of the simulation cell. We can get insight into the extent of charge localisation by plotting the planar average of the density difference between the faulted and perfect cells (middle panel) and by integrating this along the *c* axis (bottom panel). We can see the expected consistency between charge difference and potential difference.

It is clear from Fig. 5(a) that, relative to perfect material, charge accumulates on the Ga side of the SF in wz in agreement with Fig. 3. In Fig. 5(b) we see that the opposite is true in zb, with charge reducing on the Ga side of the SF and accumulating on the N side, consistent with both Fig. 4 and the change in the potential. The sign difference between the two cases occurs because the effect of a zb inclusion in wz is the exact opposite of a wz

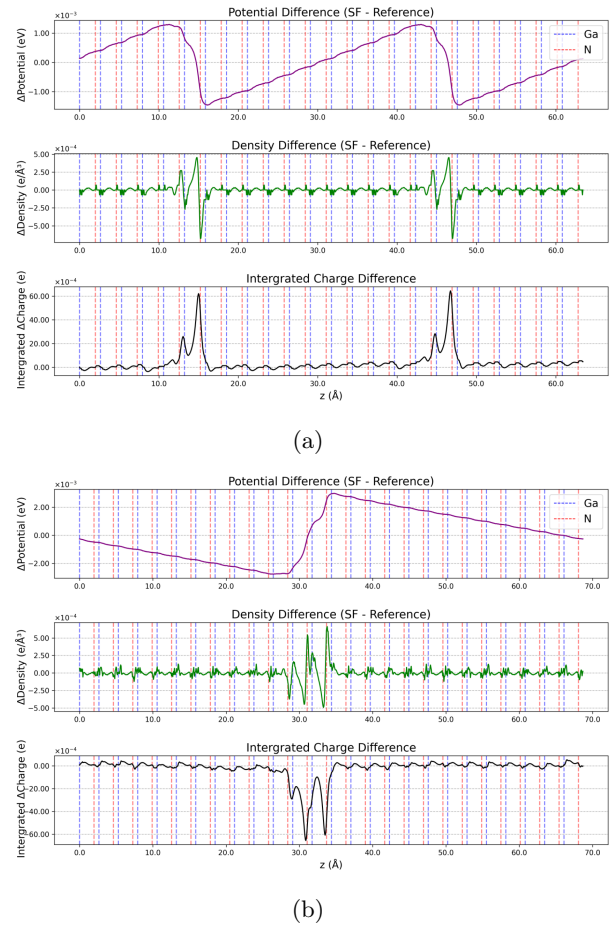


FIG. 5: Potential difference between faulted and perfect material, averaged in the x-y plane (top), density difference found in the same way (middle) and density difference integrated along z (bottom) for (a) I₁ SF in wz and (b) Intrinsic SF in zb.

inclusion in zb. (In terms of Fig. 5(a), for the potential we plot $V_{\text{Faulted}} - V_{\text{wz}}$ which in the area around the SF will be $V_{\text{zb}} - V_{\text{wz}}$; in Fig. 5(b) in the area around the SF we will effectively be plotting $V_{\text{wz}} - V_{\text{zb}}$.) The localisation of the band densities is then easily understood in terms of the potential change across the stacking faults.

It is important to understand the nature of the band alignment around the SFs (whether a type I or type II interface) as it can affect the trapping of electrons and holes and hence the optoelectronic properties[35]. We compare the band edges in simulation cells with stacking faults to cells of perfect bulk, ensuring that the deep-lying non-dispersive *d*-bands are aligned as explained in Sec. II. The band edges are shown in Fig. 6 for both wz and zb. It should be noted that, as is standard for most DFT calculations, our calculated band gaps 1.65 eV (bulk wz GaN) and 1.52 eV (bulk zb GaN) are underestimated compared to the experimental values (3.51 eV and 3.30 eV for bulk wz and zb GaN respectively[36]). This underestimate is a well-known feature of standard DFT

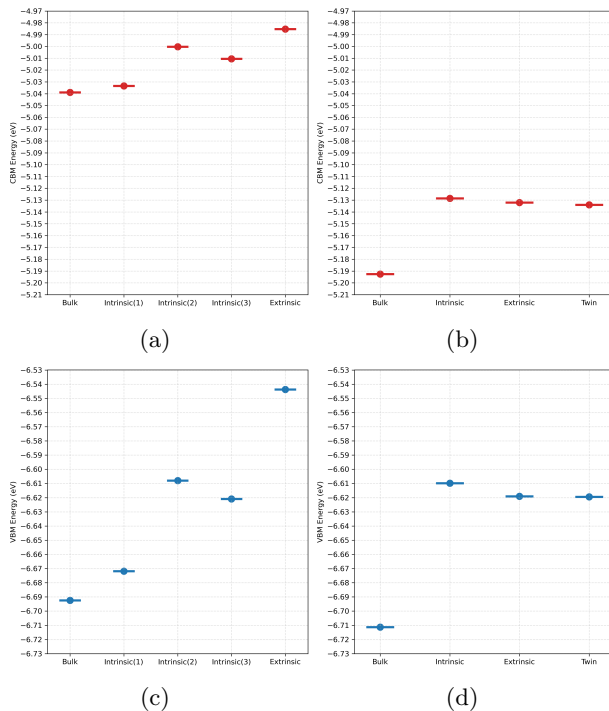


FIG. 6: Band edges: (a) WZ CBM; (b) ZB CBM; (c) WZ VBM; (d) ZB VBM.

functionals, and our calculations are in good agreement with other DFT values[16].

We see that in zb, for all SFs, these defects are type II interfaces, with both valence band maximum and conduction band minimum shifted higher than in the bulk. For wz the same is true, though for the I_1 SF (the most common) the conduction band minimum is extremely close to the energy in the bulk; the behaviour is likely to be very sensitive to local fields and perturbations of the electronic structure, so that hints type I behaviour might be seen. This is in broad agreement with existing simulation results[14, 34, 37, 38], though we are not aware of systematic testing of the size of simulation cell in other theory work. We also see that the gap is reduced by ~ 0.01 eV in the wz I_1 SF and by ~ 0.04 eV in zb I SF. Experimental CL and PL results show a similar narrowing of the gap[39] from SFs in wz samples, though the magnitude is larger, at ~ 0.9 eV.

We can further investigate the electronic properties of the stacking faults by resolving them spatially via the projected density of states (pDOS), and using this data to track the local positions of the VBM and CBM within the simulation cell. Since our focus is on the band edges, the pDOS is not shown in the main text, but is provided for all the SFs in both wz and zb in the supplementary information. In general the valence band maximum is more strongly affected than the conduction band minimum. The variation of the local band gap through the simulation cell is shown in Fig. 7 for the two most common stacking faults in wz and zb, with data for all the

other SFs given in the supplementary information. We see that the change in the gap is anti-correlated with the potential differences in Fig. 5, with the gap widening where the potential is negative. This also coincides with the location of the depletion in the valence bands, consistent with the shift of the VBM to lower energies. Calculated band gap changes ΔE_g (eV), band offsets ΔE_C (eV) and ΔE_V (eV) for the stacking faults with respect to respective bulk crystals of wz and zb GaN are presented in supporting information.

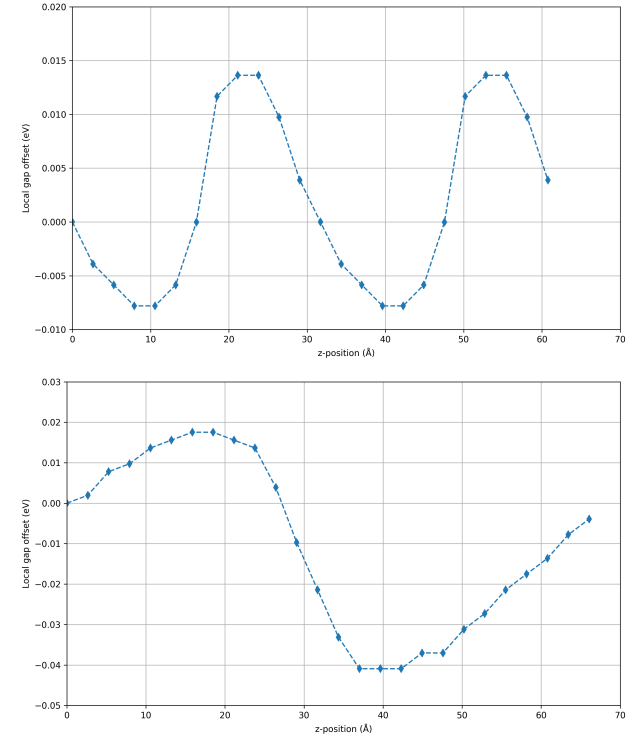


FIG. 7: Local band gap plotted across simulation cell for I_1 SF in wz GaN (a) and I SF in zb GaN (b).

V. CONCLUSIONS

We have performed a systematic study of stacking faults in wurtzite and zincblende phases of GaN using periodic DFT calculations. We have investigated all possible types of stacking faults structures, their stability and electronic properties to understand the structure properties relationship. Such investigation is of central importance since stacking faults are very common defects in III-nitride materials. From the structural relaxation, we can observe that the stacking faults have a rather small influence on lattice parameters and atomic positions; the inter-planar distance varies very slightly around the stacking faults.

The formation energies are quite low. In wz, the I_1 intrinsic stacking fault has the lowest formation energy, while all stacking faults in zb have similar energies. The

formation energy in *zb* is much smaller than that in *wz*, so stacking faults are more likely to be formed in *zb* phase compared to the *wz* phase.

The analysis of the band resolved density reveals that near the Fermi level the valence bands are concentrated on the opposite side of the stacking fault to the conduction bands. However, the concentration happens on opposite sides in *wz* and *zb*, which is understood from the fact that SFs can be seen as an inclusion of the other phase.

Finally, a detailed analysis of the electronic structure shows that the band gap of stacking faults is smaller than that of the ideal wurtzite and zincblende phases, with a positive offset. This change in the band edges is equivalent to a type II interface in all cases, though the most common *wz* stacking fault is highly sensitive.

The data that support the findings of this article are openly available[40].

ACKNOWLEDGMENTS

This research was funded through UKRI/EPSRC grant number EP/Y00423X/1. We gratefully acknowledge many useful discussions and insights from Professor Rachel Oliver, Dr Martin Frentrup, Dr Petr Vacek and Professor David Wallis of Cambridge University. This research was partly carried out using the high performance computing cluster in the London Centre for Nanotechnology. The authors acknowledge the use of the UCL Kathleen High Performance Computing Facility (KathleenUCL), and associated support services, in the completion of this work. We are grateful for computational support from the UK Materials and Molecular Modelling Hub, which is partially funded by EPSRC (EP/T022213/1, EP/W032260/1 and EP/P020194/1), for which access was obtained via the UKCP consortium and funded by EPSRC grant ref EP/P022561/1.

Supporting Information

Appendix A: Basis sets

The pseudo atomic orbital (PAO) basis sets[25] used for Ga and N were double-zeta plus polarization (DZP) basis sets, generated with the equal radius setting in Conquest. The gallium pseudopotential includes the $3d$ electrons as semi-core states, with the radii of the PAOs in Bohr as follows: $3d$: $3.58a_0$; $4s$ and $4p$: 8.06 and $4.33a_0$; $4d$ (polarization): $8.06a_0$. For N the radii are: $2s$ and $2p$: 5.48 and $2.81a_0$; $3d$ (polarization): $5.48a_0$. For indium, the pseudopotential includes the $4d$ electrons as semi-core states, with the radii of the PAOs in Bohr as follows: $4d$: $4.11a_0$; $5s$ and $5p$: 8.41 and $4.63a_0$; $5d$ (polarization): $8.41a_0$. For aluminium, the radii of the PAOs in Bohr are as follows: $3s$ and $3p$: 8.24 and $4.48a_0$; $3d$ (polarization): $8.24a_0$.

Appendix B: Physical parameters

Here we give lattice constants of the bulk, along with convergence tests for simulation cell size.

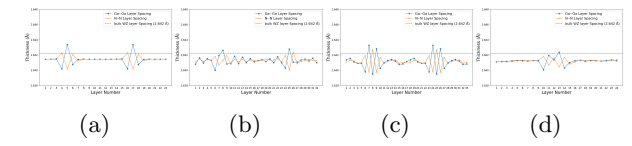


FIG. 8: Evolution of layer spacing along the *c*-axis of the simulation cell of the *wz* GaN SFs with respect to bulk *wz* GaN. I_1 (a), I_2 (b), I_3 (c) and Extrinsic (d) SFs

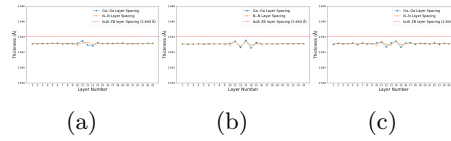


FIG. 9: Evolution of layer spacing along the *c*-axis of the simulation cell of the *ZB* GaN SFs with respect to bulk *zb* GaN. Intrinsic (a), Extrinsic (b) and Twin (c)

TABLE III: Comparison of calculated hexagonal lattice parameters a , c (\AA) of wz and cubic lattice parameter a (\AA) in zb phases of GaN, InN and AlN with available literature data.

WZ						
	a			c		
	This Study	Previous Study [41]	Exp. [32, 33]	This Study	Previous Study [41]	Exp. [31–33]
GaN	3.24	3.24	3.19	5.29	5.23	5.19
InN	3.60	3.61	3.56	5.85	5.83	5.70
AlN	3.13	3.13	3.11	5.08	5.02	4.98
Zb						
	a			c		
	This Study	Previous Study [42]	Exp. [31, 32]			
GaN	4.58	4.55	4.49			
InN	5.08	5.06	4.98			
AlN	4.42	4.40	4.37			

TABLE IV: Considered models for stacking faults, number of atoms and c parameter (\AA)

Stacking faults based on Wurtzite GaN											
I_1	Atoms	c	I_2	Atoms	c	I_3	Atoms	c	Extrinsic	Atoms	c
AB-2CB-AB	32	21.154	AB-2CA-C-AB	36	23.798	AB-C-2BA-C-AB	40	26.441	2AB-C-2AB	36	23.798
2AB-4CB-2AB	64	42.311	2AB-4CA-C-2AB	68	44.945	2AB-C-4BA-C-2AB	72	47.598	3AB-C-3AB	52	34.370
3AB-6CB-3AB	96	63.469	3AB-6CA-C-3AB	100	66.096	3AB-C-6BA-C-3AB	104	68.741	4AB-C-4AB	68	84.936
4AB-8CB-4AB	128	84.612	4AB-8CA-C-4AB	132	87.269	4AB-C-8BA-C-4AB	136	89.891	5AB-C-5AB	84	55.521
5AB-10CB-5AB	160	105.767	5AB-10CA-C-5AB	164	108.399	5AB-C-10BA-C-5AB	168	111.039	6AB-C-6AB	100	66.102
6AB-12CB-6AB	192	126.946	6AB-12CA-C-6AB	196	129.551	6AB-C-12BA-C-6AB	200	132.198	7AB-C-7AB	116	76.677
7AB-14CB-7AB	224	279.823	7AB-14CA-C-7AB	228	284.805	7AB-C-14BA-C-7AB	232	289.773	8AB-C-8AB	132	164.729
Stacking faults based on Zincblende GaN											
Intrinsic	Atoms	c	Extrinsic	Atoms	c	Twin	Atoms	c			
ABC-BC-ABC	32	39.971	ABC-B-ABC	28	34.975	ABC-BA-CABC	36	44.968			
2ABC-BC-ABC	44	54.961	2ABC-B-ABC	40	49.964	2ABC-BA-C2ABC	60	74.946			
2ABC-BC-2ABC	56	69.950	2ABC-B-2ABC	52	64.953	3ABC-BA-C3ABC	84	104.925			
3ABC-BC-2ABC	68	84.939	3ABC-B-2ABC	64	79.943	4ABC-BA-C4ABC	108	134.903			
3ABC-BC-3ABC	80	99.928	3ABC-B-3ABC	76	94.932	5ABC-BA-C5ABC	132	164.882			
4ABC-BC-3ABC	92	114.917	4ABC-B-3ABC	88	109.921	6ABC-BA-C6ABC	156	194.859			
4ABC-BC-4ABC	104	129.906	4ABC-B-4ABC	100	124.910	7ABC-BA-C7ABC	180	224.838			
5ABC-BC-4ABC	116	144.896	5ABC-B-4ABC	112	139.899						
5ABC-BC-5ABC	128	159.885	5ABC-B-5ABC	124	154.889						

TABLE V: Calculated values of formation energy (mJ/m²) of stacking faults with respect to increasing number of layers

Stacking faults based on Wurtzite GaN							
Intrinsic 1 (I ₁)	ΔE	Intrinsic 2 (I ₂)	ΔE	Intrinsic 3 (I ₃)	ΔE	Extrinsic	ΔE
AB-2CB-AB	18.627	AB-2CA-C-AB	26.806	AB-C-2BA-C-AB	34.301	2AB-C-2AB	54.989
2AB-4CB-2AB	17.058	2AB-4CA-C-2AB	26.908	2AB-C-4BA-C-2AB	34.463	3AB-C-3AB	54.711
3AB-6CB-3AB	17.051	3AB-6CA-C-3AB	27.275	3AB-C-6BA-C-3AB	35.346	4AB-C-4AB	54.643
4AB-8CB-4AB	16.709	4AB-8CA-C-4AB	27.990	4AB-C-8BA-C-4AB	35.592	5AB-C-5AB	54.918
5AB-10CB-5AB	16.546	5AB-10CA-C-5AB	27.935	5AB-C-10BA-C-5AB	35.898	6AB-C-6AB	55.270
6AB-12CB-6AB	16.936	6AB-12CA-C-6AB	28.162	6AB-C-12BA-C-6AB	36.349	7AB-C-7AB	55.357
7AB-14CB-7AB	17.123	7AB-14CA-C-7AB	28.199	7AB-C-14BA-C-7AB	36.331	8AB-C-8AB	55.426

Stacking faults based on Zincblende GaN					
Intrinsic	ΔE	Extrinsic	ΔE	Twin	ΔE
ABC-BC-ABC	-32.267	ABC-B-ABC	-31.159	ABC-BA-CABC	-34.786
2ABC-BC-ABC	-33.466	2ABC-B-ABC	-35.127	2ABC-BA-C2ABC	-36.002
2ABC-BC-2ABC	-33.567	2ABC-B-2ABC	-35.010	3ABC-BA-C3ABC	-34.804
3ABC-BC-2ABC	-33.487	3ABC-B-2ABC	-36.281	4ABC-BA-C4ABC	-34.467
3ABC-BC-3ABC	-33.470	3ABC-B-3ABC	-34.744	5ABC-BA-C5ABC	-34.190
4ABC-BC-3ABC	-33.150	4ABC-B-3ABC	-34.604	6ABC-BA-C6ABC	-33.826
4ABC-BC-4ABC	-32.934	4ABC-B-4ABC	-34.413	7ABC-BA-C7ABC	-33.494
5ABC-BC-4ABC	-32.783	5ABC-B-4ABC	-34.217		
5ABC-BC-5ABC	-34.413	5ABC-B-5ABC	-33.901		

Appendix C: Band Densities

The band densities for the I_1 stacking fault in wz GaN and the I stacking fault in zb GaN are shown in the main text. Here we show the other band densities in Figs. 10 to 14.

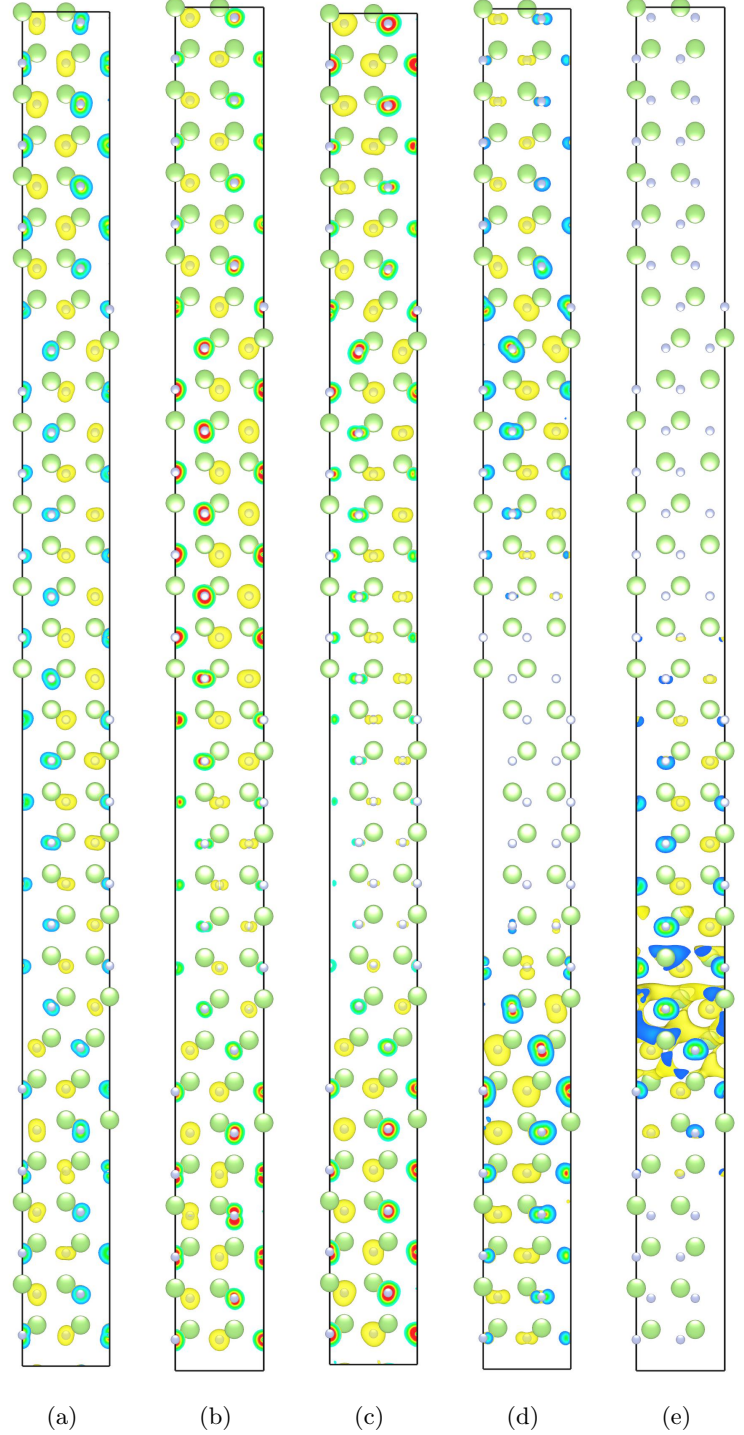


FIG. 10: Band Density of Intrinsic-2 (4AB-8CA-C-4AB) stacking fault of wz GaN. (a) Band 591, (b) Band 592, (c) Band 593, (d) Band 594, (e) Band 595, (f) Band 596, (g) Band 597, (h) Band 598. Fermi Energy (Ef: -5.86 eV) lies in between band 594 and band 595.

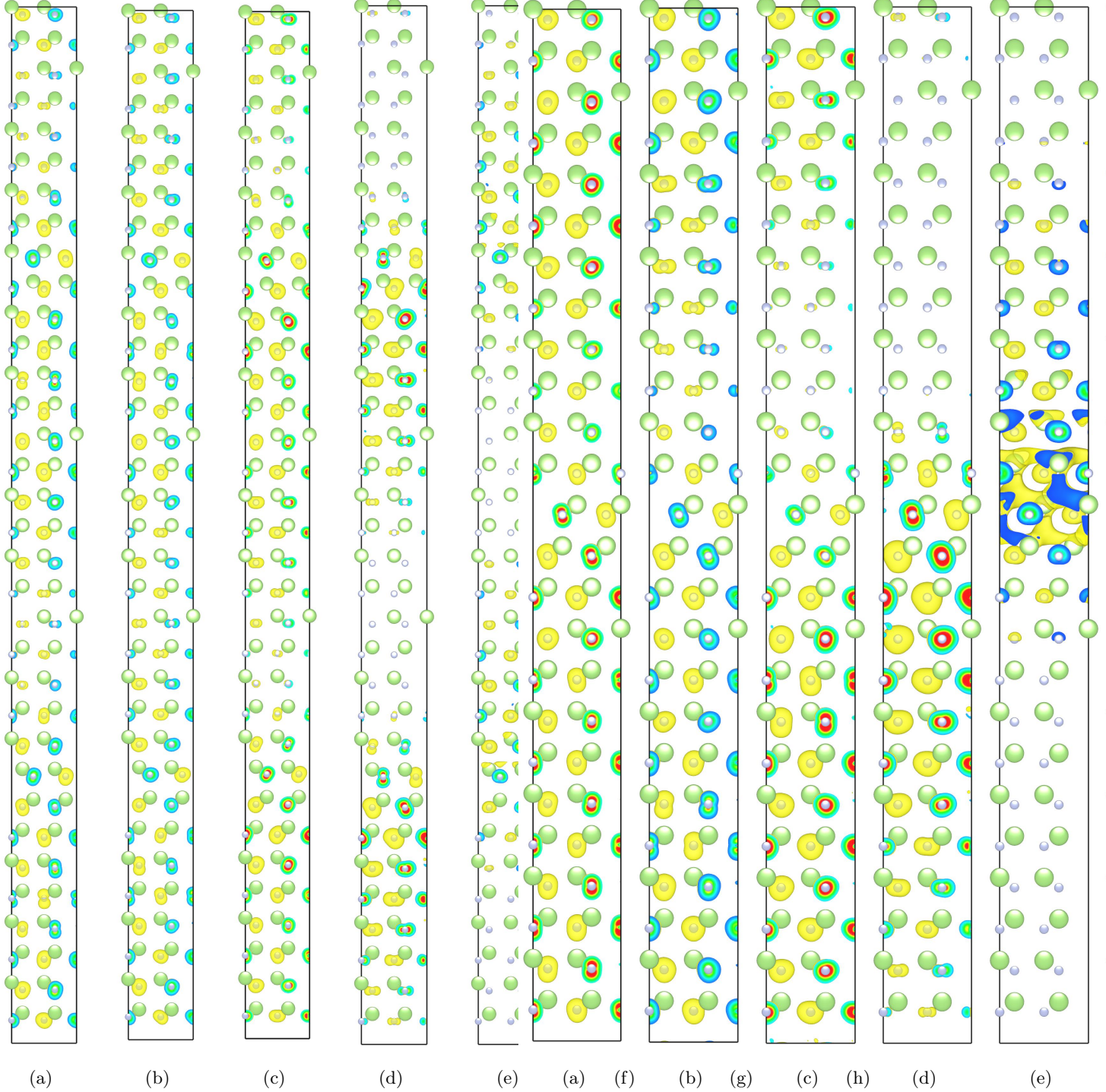


FIG. 11: Band Density of Intrinsic-3 (4AB-C-8BA-C-4AB) stacking fault of wz GaN. (a) Band 609, (b) Band 610, (c) Band 611, (d) Band 612, (e) Band 613, (f) Band 614, (g) Band 615, (h) Band 616. Fermi Energy (E_f : -5.86 eV) lies in between band 612 and band 613.

FIG. 12: Band Density of Extrinsic (6AB-C-6AB) stacking fault of wz GaN. (a) Band 447, (b) Band 448, (c) Band 449, (d) Band 450, (e) Band 451, (f) Band 452, (g) Band 453, (h) Band 454. Fermi Energy (E_f : -5.80 eV) lies in between band 450 and band 451.

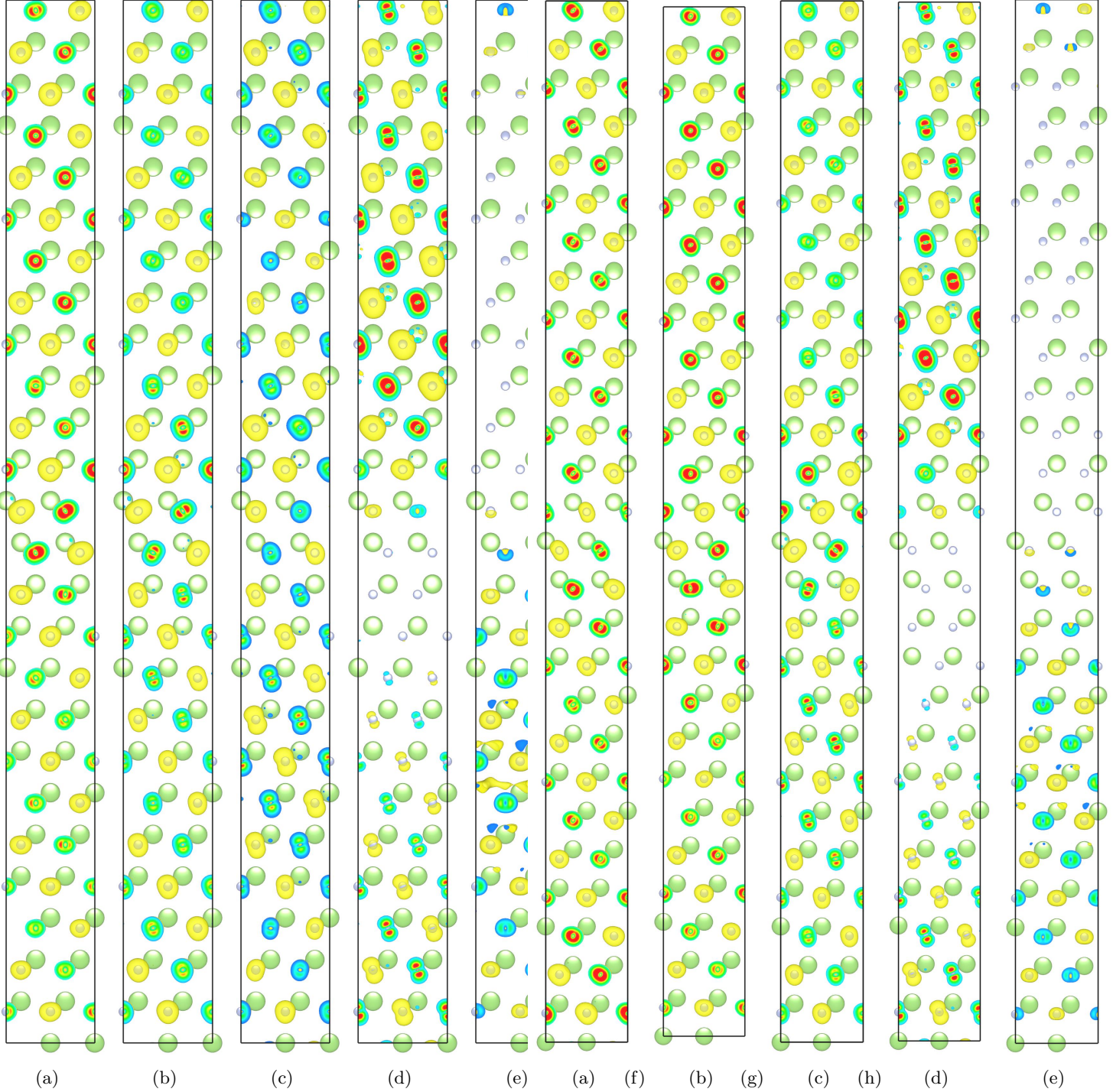


FIG. 13: Band Density of Extrinsic (4ABC-B-4ABC) stacking fault for zb GaN. (a) Band 447 , (b) Band 448 , (c) Band 449, (d) Band 450, (e) Band 451 , (f) Band 452 , (g) Band 453 , (h) Band 454. Fermi Energy ($E_F = -0.2146$ Ha) lies in between band 450 and band 451.

FIG. 14: Band density of Twin (4ABC-BAC-4ABC) stacking fault for zb GaN. (a) Band 483 , (b) Band 484 , (c) Band 485, (d) Band 486, (e) Band 487 , (f) Band 488 , (g) Band 489 , (h) Band 490. Fermi Energy ($E_F = -0.2145805742$ Ha) lies in between band 486 and band 487.

Appendix D: Potentials

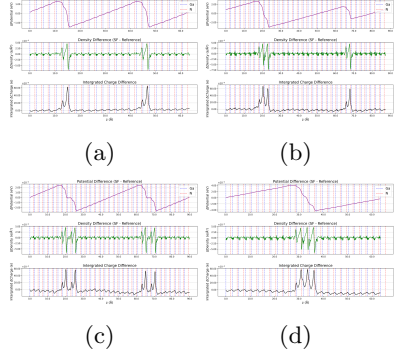


FIG. 15: Average potential of stacking faults based on wz GaN (a) I₁ (3AB-6CB-3AB) (b) I₂ (4AB-8CA-C-4AB) (c) I₃ (4AB-C-8BA-C-4AB) (d) Extrinsic (6AB-C-6AB).

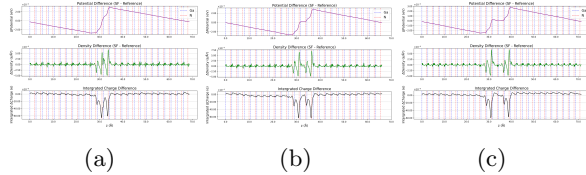


FIG. 16: Average potential of stacking faults based on zb GaN (a) intrinsic (b) extrinsic and (c) twin.

Appendix E: Projected DOS

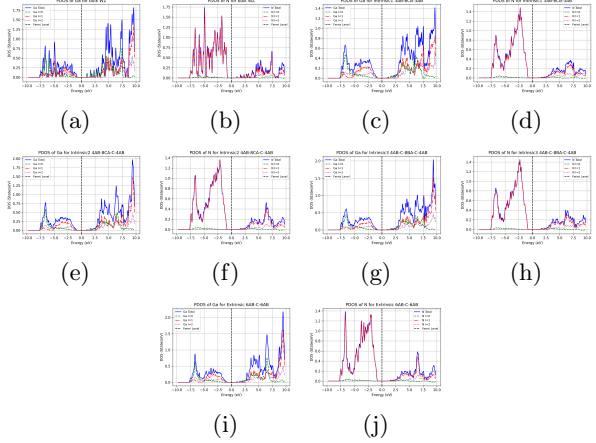


FIG. 17: Projected density of states (pDOS) for wurtzite bulk and atoms located at the SFs, showing total (blue) and decomposed by angular momentum: (a) and (b) bulk (Ga and N respectively); (c) and (d) I_1 SF (Ga and N respectively); (e) and (f) I_2 SF (Ga and N respectively); (g) and (h) I_3 SF (Ga and N respectively); (i) and (j) Extrinsic SF (Ga and N respectively).

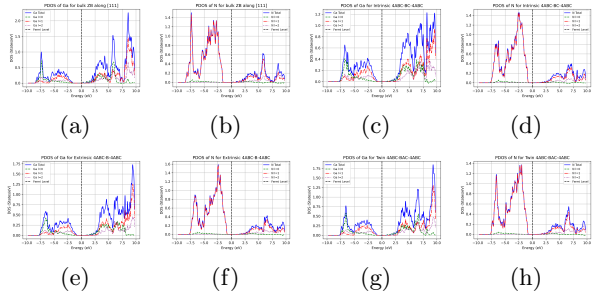


FIG. 18: Projected density of states (pDOS) for zincblende bulk and atoms located at the SFs, showing total (blue) and decomposed by angular momentum: (a) and (b) bulk (Ga and N respectively); (c) and (d) intrinsic SF (Ga and N respectively); (e) and (f) extrinsic SF (Ga and N respectively); (g) and (h) twin SF (Ga and N respectively).

Appendix F: Band Gap Changes

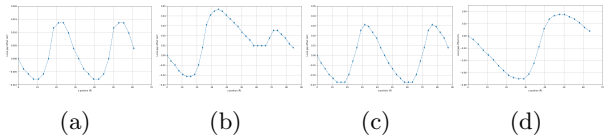


FIG. 19: Band gap evolution along c-axis of simulation cell for stacking faults in wz GaN. I₁ (a), I₂ (b), I₃ (c) and Extrinsic (d)

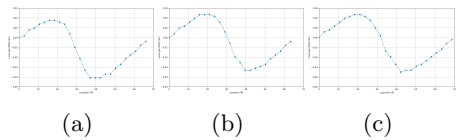


FIG. 20: Band gap evolution along c-axis of simulation cell for stacking faults of zb GaN. Intrinsic (a), Extrinsic (b) and Twin (c).

TABLE VI: Calculated values of band gap difference ΔE_g (eV), band offsets ΔE_C (eV) and ΔE_V (eV) for the stacking faults with respect to ideal crystals of wz and zb GaN

Stacking faults based on Wurtzite GaN				
	Intrinsic 1 (I ₁)	Intrinsic 2 (I ₂)	Intrinsic 3 (I ₃)	Extrinsic
ΔE_g	-0.015 (-0.050[16])	-0.046 (-0.120[16])	-0.043	-0.095 (-0.140[16])
ΔE_C	0.005 (-0.045[16])	0.039 (-0.096[16])	0.028	0.054(-0.160[16])
ΔE_V	0.021(0.011[16])	0.085 (0.019[16])	0.071	0.149(0.028[16])
Stacking faults based on Zincblende GaN				
	Intrinsic	Extrinsic	Twin	
ΔE_g	-0.037	-0.032	-0.033	
ΔE_C	0.064	0.060	0.059	
ΔE_V	0.101	0.092	0.092	

[1] B. Ding, Mater. Sci. Technol. **34**, 1615 (2018).

[2] T. Ito, T. Araki, T. Akiyama, and K. Nakamura, J. Crys. Growth **301**, 62 (2007).

[3] S. Lester, F. A. Ponce, M. G. Crawford, and D. A. Steigerwald, Appl. Phys. Lett. **66**, 1249 (1995).

[4] M. Barchuk, V. Holý, D. Kriegner, J. Stangl, S. Schwaiger, and F. Scholz, Phys. Rev. B **84**, 094113 (2011).

[5] F. Bernardini, V. Fiorentini, and D. Vanderbilt, Phys. Rev. B **56**, R10024 (1997).

[6] H. Morkoç, R. Cingolani, W. Lambrecht, B. Gil, H.-X. Jiang, J. Lin, D. Pavlidis, and K. Shenai, MRS Internet J. Nitride Semic. Res. **4**, 18 (1999).

[7] A. Trampert, O. Brandt, H. Yang, and K. Ploog, Appl. Phys. Lett. **70**, 583 (1997).

[8] D. Binks, P. Dawson, R. Oliver, and D. Wallis, Appl. Phys. Lett. **9**, 041309 (2022).

[9] B. Ding, M. Frentrup, S. Fairclough, M. Kappers, M. Jain, A. Kovács, D. Wallis, and R. Oliver, J. Appl. Phys. **128** (2020).

[10] Z. Liliental-Weber, M. Benamara, J. Washburn, I. Grzegory, and S. Porowski, Phys. Rev. Lett. **83**, 2370 (1999).

[11] T. Schmidt, R. Miwa, W. Orellana, and H. Chacham, Phys. Rev. B **65**, 033205 (2002).

[12] J. Lähnemann, U. Jahn, O. Brandt, T. Flissikowski, P. Dogan, and H. T. Grahn, J. Phys. D: Appl. Phys. **47**, 423001 (2014).

[13] E. Yücelen, I. Lazić, and E. G. Bosch, Sci. Rep. **8**, 2676 (2018).

[14] C. Stampfl and C. G. Van de Walle, Phys. Rev. B **59**, 5521 (1999).

[15] I. Batyrev, W. Sarney, T. Zheleva, C. Nguyen, B. Rice, and K. Jones, phys. stat. sol. a **208**, 1566 (2011).

[16] A. Benbedra, S. Meskine, A. Boukortt, R. Hayn, M. Texier, O. Thomas, and T. W. Cornelius, Comp. Cond. Matter **43**, e01033 (2025).

[17] Z. Antoš, P. Vacek, and R. Gröger, Comput. Mater. Sci. **180**, 109620 (2020).

[18] H. Xiu, S. M. Fairclough, A. Gundimeda, M. J. Kappers, D. J. Wallis, R. A. Oliver, and M. Frentrup, J. Appl. Phys. **133** (2023).

[19] Bowler, D R and Miyazaki, T and Gillan, M J, J. Phys. Condens. Matter **14**, 2781 (2002).

[20] T. Miyazaki and D. R. Bowler and R. Choudhury and M. J. Gillan, J. Chem. Phys. **121**, 6186 (2004).

[21] A. Nakata, J. S. Baker, S. Y. Mujahed, J. T. L. Poulton, S. Arapan, J. Lin, Z. Raza, S. Yadav, L. Truflandier, T. Miyazaki, and D. R. Bowler, *The Journal of Chemical Physics*, J. Chem. Phys. **152**, 164112 (2020).

[22] J. P. Perdew, K. Burke, and M. Ernzerhof, Phys. Rev. Lett. **77**, 3865 (1996).

[23] D. R. Hamann, Phys. Rev. B **88**, 085117 (2013).

[24] M. J. van Setten, M. Giantomassi, E. Bousquet, M. J. Verstraete, D. R. Hamann, X. Gonze, and G. M. Rignanese, Comp. Phys. Commun. **226**, 39 (2018).

[25] D. R. Bowler, J. S. Baker, J. T. L. Poulton, S. Y. Mujahed, J. Lin, S. Yadav, Z. Raza, and T. Miyazaki, Jap. J. Appl. Phys. **58**, 100503 (2019).

[26] B. Schaefer, S. Alireza Ghasemi, S. Roy, and S. Goedecker, J. Chem. Phys. **142**, 034112 (2015).

[27] The stacking sequence of the layers in bulk GaN are often notated AaBb (wz) and AaBbCc (zb) with Aa indicating the alternation of planes of Ga and N along the (0001) direction (wz) or (111) direction (zb). We will shorten this to AB and ABC respectively for simplicity of notation.

[28] D. N. Zakharov, Z. Liliental-Weber, B. Wagner, Z. J. Reitmeier, E. A. Preble, and R. F. Davis, Phys. Rev. B **71**, 235334 (2005).

[29] M. Moram and M. Vickers, Rep. Prog. Phys. **72**, 036502 (2009).

[30] M. Moram, C. Johnston, J. Hollander, M. Kappers, and C. Humphreys, J. Appl. Phys. **105** (2009).

[31] M. Frentrup, L. Y. Lee, S.-L. Sahonta, M. J. Kappers, F. Massabuau, P. Gupta, R. A. Oliver, C. J. Humphreys, and D. J. Wallis, J. Phys. D: Appl. Phys. **50**, 433002 (2017).

[32] B. Ding, *Study of wurtzite and zincblende GaN based green LED heterostructure*, Ph.D. thesis, University of Cambridge (2021).

[33] H. Schulz and K. Thiemann, Solid State Commun. **23**, 815 (1977).

[34] J. Lähnemann, O. Brandt, U. Jahn, C. Pfüller, C. Roder, P. Dogan, F. Grosse, A. Belabbes, F. Bechstedt, A. Trampert, and L. Geelhaar, Phys. Rev. B **86**, 081302 (2012).

[35] M. A. Caro, S. Schulz, and E. P. O'Reilly, Phys. Rev. B **88**, 214103 (2013).

[36] I. Vurgaftman and J. R. Meyer, J. Appl. Phys. **94**, 3675 (2003).

[37] X. H. Lu, P. Y. Yu, L. X. Zheng, S. J. Xu, M. H. Xie, and S. Y. Tong, Appl. Phys. Lett. **82**, 1033 (2003).

[38] Y. J. Sun, O. Brandt, U. Jahn, T. Y. Liu, A. Trampert, S. Cronenberg, S. Dhar, and K. H. Ploog, J. Appl. Phys. **92**, 5714 (2002).

[39] M. Häberlen, T. J. Badcock, M. A. Moram, J. L. Hollander, M. J. Kappers, P. Dawson, C. J. Humphreys, and R. A. Oliver, J. Appl. Phys. **108**, 033523 (2010).

[40] Z. Wang, M. Islam, and D. R. Bowler, <https://doi.org/10.5281/zenodo.18259436> (2026).

[41] Y. Gao, D. Sun, X. Jiang, and J. Zhao, J. Appl. Phys. **125**, 215705 (2019).

[42] L. C. De Carvalho, A. Schleife, and F. Bechstedt, Phys. Rev. B **84**, 195105 (2011).